An Investigation on Analytical Methods for Correction of Distance-Dependent Resolution Variation in 3D SPECT Imaging [1)]

Jian Li, Zhengrong Liang, Jinghan Ye, and Guoping Han

Abstract— **Spatial resolution variation as a function of distance from collimator surface in single photon emission computed tomography (SPECT) is a major obstacle for quantitative imaging. This work investigated two analytical inversion methods for correcting the distance-dependent resolution variation. The first one derives accurately an inversion formula, but approximates the resolution variation kernel. The second one considers accurately the resolution variation kernel, but approximates the inversion formula. Reconstructed images using the first method showed a better resolution recovery at the central area of field-of-view (FOV), consistent with the approach that the resolution kernel is approximated for near-field regions. The second method restored resolution better at the FOV periphery, consistent with the theory that the formula is approximated for far-field regions. The first method is very sensitive to the approximation. The second one is robust and, therefore, is a better choice for quantitative SPECT imaging.**

I. INTRODUCTION

SPECT is a non-invasive cost-effective means for assessment of tissue/organ functions in nuclear medicine [1]. Currently available SPECT technology provides only qualitative images of radiotracer uptake in regions-of-interest (ROIs) and lacks of quantitative capability. The spatial resolution variation as a function of distance from the collimator surface is one of the major obstacles for quantitative imaging, in addition to photon attenuation (absorption and scatter) in the body [2]. This work investigates two inversion methods for correcting the distance-dependent resolution variation.

The first method derives accurately the inversion formula, but approximates the resolution kernel to some special functional forms to satisfy the mathematical derivation [3]. The approximation introduces incorrect information of the kernel into the near-field regions. The second method considers accurately the resolution kernel constructed from point-source measurements at different distances from the collimator surface, but approximates the inversion formula [4]. The approximation compromises the information in the far-field regions. The goal of this work is to study their performance and recommend a better choice.

[1)] This work was supported by NIH Grant #HL54166 of the National Heart, Lung, and Blood Institute; Grant #NS53833 of the National Institute of Neurological Disorders and Strok; Grant #CA79180 of the National Cancer Institute; and Established Investigatorship of the American Heart Association.

The authors are with the Departments of Radiology, Computer Science, and Physics and Astronomy, State University of New York, Stony Brook, NY 11794

II. METHOD

Projection equation for SPECT imaging with parallel-hole collimation is given, if scatter contribution is neglected or removed, see Figure 1 [5],

$$\tilde{p}(\xi,z,\theta) = \iiint_{-\infty}^{\infty} h(\xi-\xi',z-z',\eta)o(\xi',z',\eta,\theta) \times e^{-\int_{-\infty}^{\eta}\mu(\xi',z',\eta',\theta)d\eta'}d\xi'dz'd\eta \quad (1)$$

where $o(\xi,z,\eta,\theta)$, $\mu(\xi,z,\eta,\theta)$ and $h(\xi,z,\eta)$ represent the source (radiotracer) distribution $o(x,y,z)$, the attenuation map $\mu(x,y,z)$ and the resolution-variation kernel in the rotation coordinates (ξ,z,η), and $\tilde{p}(\xi,z,\theta)$ is the (scatter corrected or free) measurement at detection bin (ξ,z,θ) by projection angle θ. It can be seen that the integrals for ξ' and z' on the $\xi-z$ plane at a constant distance η is a convolution of attenuated source with the resolution kernel. Efficient inversion of Eq.(1) for $o(x,y,z)$ can be performed either analytically if radiotracer distributes inside a uniform attenuating medium or iteratively if the tracer is within nonuniform attenuating body.

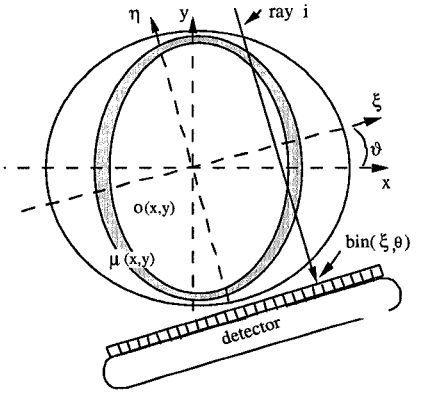

Figure 1. Data acquisition configuration for SPECT imaging. The z-axis is the rotation axis.

Let ν be the attenuation coefficient of the uniform medium. By multiplying attenuation factor, $e^{-\int_{-\infty}^{0}\mu(\xi',z',\eta',\theta)d\eta'}$, to both sides of Eq.(1), we have

$$\hat{p}(\xi,z,\theta) = \iiint_{-\infty}^{\infty} h(\xi-\xi',z-z',\eta)o(\xi',z',\eta,\theta) \times e^{-\nu\eta}\mathrm{d}\xi'\mathrm{d}z'\mathrm{d}\eta. \quad (2)$$

By applying a two-dimensional (2D) Fourier transform

0-7803-5021-9/99/$10.00 (c) 1999 IEEE

(FT) to $\widehat{p}(\xi, z, \theta)$ on the ξ-z detection plane, we have

$$\widehat{P}(f_\xi, f_z, \theta) = \iiint_{-\infty}^{\infty} o(\xi, z, \eta, \theta) H(f_\xi, f_z, \eta) \times e^{-2\pi i(f_\xi \xi + f_z z) - \nu\eta} \mathrm{d}\xi \mathrm{d}z \mathrm{d}\eta \quad (3)$$

where $H(f_\xi, f_z, \eta)$ is the 2D FT of the resolution kernel $h(\xi, z, \eta)$ at distance η, with f_ξ being the spatial frequency along ξ-axis and f_z the spatial frequency along z-axis.

A. Approximation of resolution kernel for accurate inversion formula

Assume that the FT of the resolution kernel can be written as

$$H(f_\xi, f_z, \eta) = g(f_\xi, f_z) e^{-\tau(f_\xi, f_z)\eta} \quad (4)$$

to fit approximately the measured kernel. Substitute this into Eq.(3) and divide $g(f_\xi, f_z)$ to both sides, we have

$$P(f_\xi, f_z, \theta) = \iiint_{-\infty}^{\infty} e^{-2\pi i(f_\xi \xi + f_z z) - (\nu+\tau)\eta} \times o(\xi, z, \eta, \theta) \mathrm{d}\xi \mathrm{d}z \mathrm{d}\eta. \quad (5)$$

Let $\alpha = \frac{\nu+\tau}{2\pi}$. By the transformation of $f_\xi = \rho\cos\beta$ and $-i\alpha = \rho\sin\beta$ [6], where ρ is a real variable and β is an imaginary one, Eq.(5) becomes

$$P(f_\xi, f_z, \theta) = O[\rho\cos(\theta+\beta), \rho\sin(\theta+\beta), f_z] \quad (6)$$

where $\beta = \frac{i}{2}\ln\frac{f_\xi - \alpha}{f_\xi + \alpha}$ and $O(.)$ is the 3D FT of $o(x, y, z)$.

$P(f_\xi, f_z, \theta)$ is a periodic function of $\theta + 2\pi$, and so is $O(.)$ for $\theta + \beta + 2\pi$. By applying the Fourier series expansion to both sides of Eq.(6) with respect to the angular variables, the inversion formula is then written as [5][6]

$$O_n(\rho, f_z) = P_n(f_\xi, f_z) \left(\frac{f_\xi - \alpha}{f_\xi + \alpha}\right)^{\frac{n}{2}} \quad (7)$$

where $P_n(f_\xi, f_z)$ is the FT of $P(f_\xi, f_z, \theta)$ on the angular coordinate θ and $O_n(\rho, f_z)$ is the 3D FT of the attenuation-compensated and resolution-restored projections, which are to be obtained from Eq.(7) and used to reconstruct the source distribution $o(x, y, z)$. Index n is the angular frequency and ρ is given by [7]

$$\rho = \sqrt{f_\xi^2 - \alpha^2} \text{ if } f_\xi \geq 0; \quad \rho = -\sqrt{f_\xi^2 - \alpha^2} \text{ if } f_\xi < 0. \quad (8)$$

Given the attenuation map $\mu(x, y, z)$ with central uniform attenuating medium of convex region and the resolution kernel $h(\xi, z, \eta)$ satisfying Eq.(4), the source distribution $o(x, y, z)$ within the central uniform attenuating medium is determined, in the frequency space, by the analytical inversion Eqs.(7) and (8). The implementation of the analytical inversion is detailed below.

A.1 Approximated Gaussian resolution kernel

Assume the resolution kernel to be Gaussian functional with the variance σ_η^2 depending on the distance η, i.e.,

$$h(\xi, z, \eta) = \frac{1}{2\pi\sigma_\eta^2} e^{-\frac{\xi^2+z^2}{2\sigma_\eta^2}} \quad (9)$$

then the 2D FT of the kernel on the ξ-z plane is given by

$$H(f_\xi, f_z, \eta) = e^{-2\pi^2\sigma_\eta^2(f_\xi^2 + f_z^2)}. \quad (10)$$

The relation $\sigma_\eta = \sigma_o(1 + \gamma\eta)$ is usually satisfied, with the standard deviation σ_o being the FWHM (full-width-at-half-maximum) at the plane ($\eta = 0$) and γ being a positive constant reflecting the rate of FWHM change as a function of η. In order to analytically inverting Eq.(2), however, a linear dependence of $\sigma_\eta^2 \approx a\eta + b$, where a and b are positive constants, is required to satisfy Eq.(4) [3] [8][9]. Using this approximation, $H(f_\xi, f_z, \eta)$ becomes

$$H(f_\xi, f_z, \eta) = e^{-2\pi^2 b(f_\xi^2 + f_z^2)} e^{-2\pi^2 a(f_\xi^2 + f_z^2)\eta}. \quad (11)$$

The relationship between f_ξ, ρ and f_z is determined via Eq.(8) and $\alpha = \frac{\nu+\tau}{2\pi}$:

$$f_\xi = \pm\sqrt{\frac{(1 - a\nu) - \sqrt{1 - 2a\nu - (2a\pi)^2(f_z^2 + \rho^2)}}{2(a\pi)^2} - f_z^2}. \quad (12)$$

From this equation, given f_z and ρ, we can solve f_ξ. Then the solution $o(x, y, z)$ is obtained via Eq.(7).

A.2 Approximated Cauchy resolution kernel

Other approximations by selecting a non-Gaussian functional $h(\xi, z, \eta)$ to satisfy Eq.(4) have also been explored, e.g., a Cauchy function [8][9]:

$$h(\xi, z, \eta) = \frac{\sigma_\eta}{\pi} \frac{1}{\xi^2 + z^2 + \sigma_\eta^2}. \quad (13)$$

The 2D FT on the ξ-z plane is given by

$$H(f_\xi, f_z, \eta) = e^{-2\pi b_c\sqrt{f_\xi^2 + f_z^2}} e^{-2\pi a_c\sqrt{f_\xi^2 + f_z^2}\eta} \quad (14)$$

where it has been assumed that $\sigma_\eta^2 = a_c\eta + b_c$. The relationship between f_ξ, ρ and f_z is:

$$f_\xi = \pm\sqrt{\frac{2\omega^2 + \frac{(a_c\nu)^2}{\pi^2} + \frac{a_c\nu}{\pi}\sqrt{\frac{(a_c\nu)^2}{\pi^2} + 4\omega^2}}{2(1 - a_c^2)^2} - f_z^2} \quad (15)$$

where

$$\omega^2 = (1 - a_c^2)\left[f_z^2 + \rho^2 + \frac{\nu^2}{(2\pi)^2}\right].$$

From this equation, we determine f_ξ, given samples f_z and ρ. Then we compute the solution $o(x, y, z)$ by Eq.(7).

The square-root part in Eq.(12) must be positive, giving the maximum frequency radius of ρ -f_z

$$\frac{\sqrt{1 - 2a\nu}}{2a\pi}. \quad (16)$$

Eq.(16) eliminates those high frequencies for f_z and ρ when computing $O_n(\rho, f_z)$ via Eq.(7). This is the limitation of the approximated Gaussian resolution kernel. The loss of information in those high frequency can result in reconstruction artifacts. For the Cauchy resolution kernel, the square-root part in Eq.(15) is always greater than 0, since $a_c < 1$. Therefore, Cauchy kernel does not lose the information in those high frequencies and should outperform the Gaussian kernel.

0-7803-5021-9/99/$10.00 (c) 1999 IEEE

A.3 Inversion solution via Eq.(7)

The attenuation-compensated and resolution-restored projections $O_n(\rho, f_z)$ are computed via Eqs.(7) and (8). For the linearly approximated Gaussian kernel, Eq.(12) will be used. When the Cauchy kernel is considered, Eq.(15) will be applied. According to the symmetric properties of the 3D FT of a real 3D function, we have [5]:

$$O_n(\rho, -f_z) = (-1)^n O_n^*(\rho, f_z) \tag{17}$$

$$O_{-n}(\rho, f_z) = (-1)^n O_n^*(\rho, -f_z)$$

$$O_{-n}(-\rho, f_z) = O_n^*(\rho, -f_z)$$

$$O_{-n}(-\rho, -f_z) = O_n^*(\rho, f_z).$$

For noise-free case, two more symmetries for computing O_n values are available:

$$O_n(-\rho, f_z) = (-1)^n O_n(\rho, f_z) \tag{18}$$

$$O_n(-\rho, -f_z) = (-1)^n O_n(\rho, -f_z).$$

A.4 Frequency Sampling

Assume that in the space domain, the sampling number in ξ direction is N and in z direction is S, all having the same sampling interval T. To avoid interpolation in frequency space, the sampled frequencies are expressed as:

$$\begin{array}{ll} \rho_l = \frac{l+\frac{1}{2}}{NT}, & l = -\frac{N}{2}, -\frac{N}{2}+1, ..., 0, 1, ...\frac{N}{2}-1; \\ (f_z)_m = \frac{m}{ST}, & m = -\frac{S}{2}, -\frac{S}{2}+1, ..., 0, 1, ..., \frac{S}{2}-1. \end{array} \tag{19}$$

Notice that the pair l and n run only half $\{l = 0, 1, ..., \frac{N}{2} - 1;\ \ n = 0, 1, ..., \frac{N}{2} - 1\}$ for $O_n(l, m)$. The other quarters $\{l = -\frac{N}{2}, ..., -1;\ \ n = -\frac{N}{2}, ..., -1\}$ can be obtained by the symmetries of Eqs.(17)-(18).

A.5 Filtered Backprojection (FBP) Reconstruction

Given $O_n(l, m)$, an inverse FT on the angular index n produces the attenuation-compensated and resolution-restored projections in frequency space (f_ξ, f_z) at different projection angle θ: $P(f_\xi, f_z, \theta, \mu = 0, h = \delta)$. A 2D Ramp filter is applied on the f_ξ-f_z plane and then a backprojection is performed for each angle θ to reconstruct the source distribution $o(x, y, z)$.

B. Accurate consideration of resolution kernel for approximated inversion formula

Based on a central-ray approximation and the distance-frequency relation [4], inversion of Eq.(2) for solution $o(x, y, z)$ can be performed sequentially [10], rather than simultaneously as described above.

Step (1) is a distance-dependent deconvolution based on the distance–frequency relation:

$$P(f_\xi, f_z, f_\theta) = \frac{\widehat{P}(f_\xi, f_z, f_\theta)}{H(f_\xi, f_z, -f_\theta/f_\xi) + c}, \tag{20}$$

where f_θ is the angular frequency of θ and c is a small constant.

Step (2) performs the inversion of exponential Radon transform based on FBP reconstruction [7].

The first method described in Section A derives accurately the inversion method of Eq.(7) with approximated kernels of Eq.(4). The second method described in Section B approximates the inversion formula of Eq.(20), based on the distance-frequency relation, and considers accurately the measured kernel. The goal of this work is to compare the performances of the approximated resolution kernel of Eq.(4) and the approximated inversion formula of Eq.(20) in image reconstruction.

III. RESULT

A study on noise-free data was performed by computer simulations and followed by an investigation on noisy data with phantom experiments.

A. Simulation results

Figure 2 shows a slice of the 3D Hoffman brain phantom and a horizontal profile across the image center. Projection data were simulated by parallel-hole collimation. A circular scanning orbit was used with 128 evenly spaced views. Each view took a projected image of 128×128 array. A uniform attenuation was included. An experimentally measured resolution kernel of an LEUR (low energy ultra-high resolution) parallel-hole collimator was used.

Figure 3 shows the reconstruction without correction of the distance-dependent resolution variation. The blurring is clearly seen from the profile.

Figure 4 shows the result after resolution correction using the first method [3] with approximated resolution kernel of Cauchy form. The Cauchy kernel has the same FWHM σ_η as the measured kernel. Improvement in resolution recovery is seen in the profile. Reconstruction artifacts can be observed near the *hot* spot. This is due to the mismatch of Cauchy function to the measured kernel. Figure 5 shows the result of the first method [3] with approximated resolution kernel of Gaussian function (linear variation). The linear fitting of $\sigma_\eta^2 = a\eta + b$ to the point-source measurements was performed by the technique [3]. The profile shows the resolution recovery. Due to the noticeable deviation of the linear fitting to the non-linear variation of measured FWHMs, reconstruction artifact is clearly seen.

In order to ensure that the first method is correctly implemented, we performed another simulation, in which the projections were simulated using the linearly approximated Gaussian kernel. The reconstruction also used the linearly approximated Gaussian kernel. The results are shown in Figure 6. A *perfect* resolution recovery is achieved (see the *hot* and *cold* sports). This indicates that the implementation is correct.

Figure 7 shows the result after resolution correction using the second method [4], i. e., accurate use of the kernel with approximated inversion formula. The profile demonstrate the improvement of resolution. The reconstruction is artifact free. This indicates that accurate consideration of the measured resolution kernel is necessary.

0-7803-5021-9/99/$10.00 (c) 1999 IEEE

The reconstructions using approximated kernels showed excellent resolution recovery at the FOV central area, but generated artifacts off the center, as indicated in Figures 4 and 5. This is consistent with the approach that the kernel is approximated for the near-field regions. The reconstructions using approximated inversion formula showed a better resolution recovery at phantom periphery, as seen in Figure 7. This is consistent with the theory that the formula is approximated for the far-field regions.

Compared to Figure 6, which is the *perfect* reconstruction because the same kernel is used for both data generation and image reconstruction, the result of Figure 7 is *nearly perfect*. Most importantly, it is artifact free.

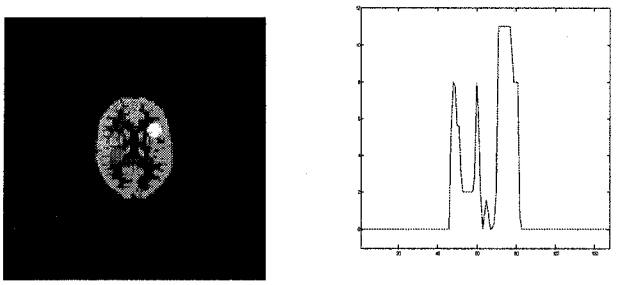

Figure 2. A slice of the 3D Hoffman phantom.

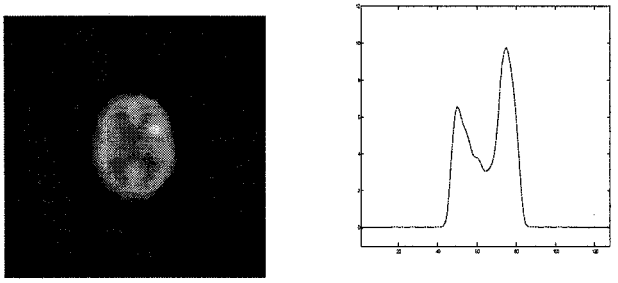

Figure 3. Reconstruction without resolution variation correction.

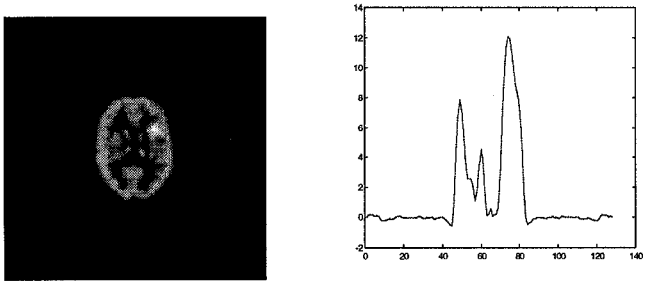

Figure 4. Reconstruction using the first method with Cauchy function as the kernel.

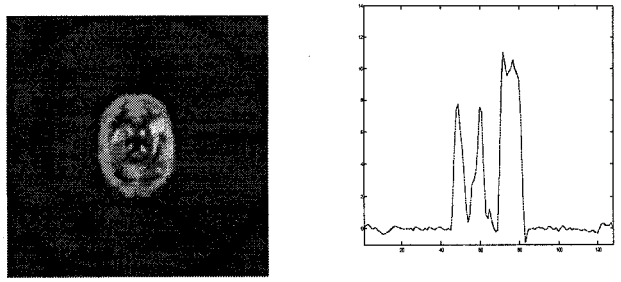

Figure 5. Reconstruction using the first method with Gaussian function as the kernel.

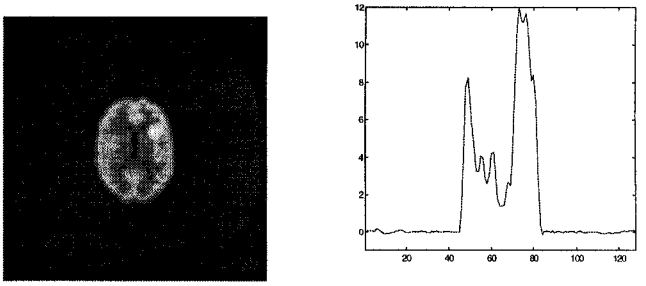

Figure 6. Reconstruction and data simulation using the same Gaussian resolution kernel.

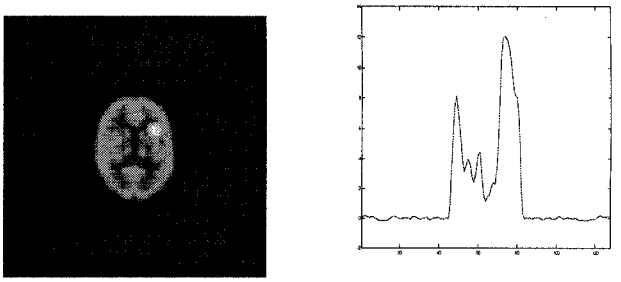

Figure 7. Reconstruction using the second method.

B. Experimental results

A Picker 3000XP SPECT system with LEUR parallel-hole collimators was used to acquire 128 projections evenly spaced on a circular orbit. Each projection is an image of 128 × 128 array. The phantom is the striatal head model (Radiology Support Devices, Inc., CA). Within a skull/scalp enclosure, this anthropomorphic phantom has 4 spots in the brain tissue space.

The reconstruction without correction for the resolution blurring is shown in Figure 8. The slice image contains 2 hot spots. The profile was drawn vertically through the spots. Figures 9 and 10 show the results of the first method [3] with approximated Cauchy and Gaussian kernels, respectively. The approximated Cauchy and Gaussian kernels were obtained by fitting their functional forms to the point-source measurements of the Picker collimators. Figure 11 shows the result after correction by the second method [4], where the measured kernel for the Picker collimators was used. In the presence of noise, the approximation of resolution kernel results in the same reconstruction artifacts as the noise-free case, see Figures 4, 5, 9 and 10. Necessity of accurate consideration of the measured resolution kernel is seen again. The second method demonstrated robust performance in both the noise-free and noisy cases. Therefore, the second method is a better choice for quantitative SPECT imaging.

IV. CONCLUSION

We have investigated two analytical inversion methods for correction of resolution variation as a function of distance from the collimator surface. The first method fits the reconstruction kernel to some special functional forms to satisfy the derivation of accurate inversion formula [3]. The fitting introduces reconstruction artifacts. The second method derives an approximated inversion formula, based

0-7803-5021-9/99/$10.00 (c) 1999 IEEE

on the distance-frequency relation [4], and considers the resolution kernel accurately. Both computer simulations and phantom experiments showed that the first method achieves excellent resolution restoration at the central region of FOV, at the cost of reconstruction artefact because of the approximation at the near-field regions. The second method recovers resolution better at the phantom periphery because of the approximation at the far-field regions. The second method demonstrated robust performance and is a better choice for resolution restoration.

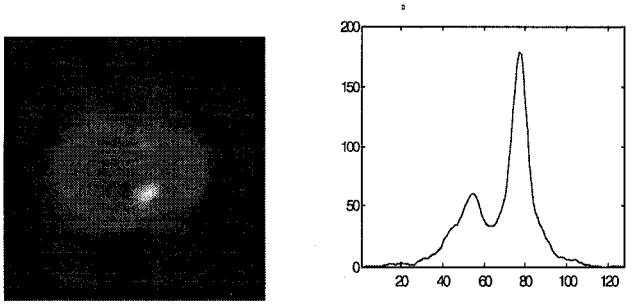

Figure 8. Reconstruction without resolution variation correction.

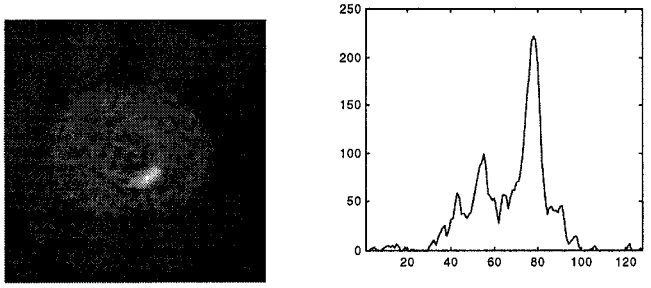

Figure 9. Reconstruction using the first method with Cauchy function as the kernel.

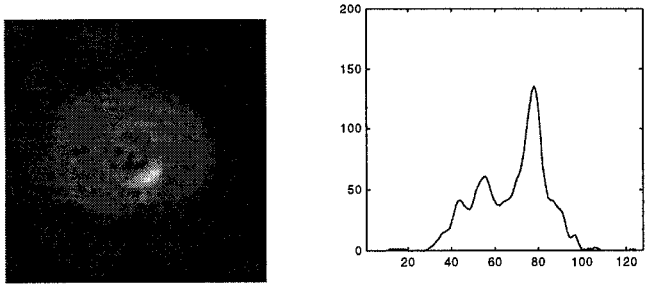

Figure 10. Reconstruction using the first method with Gaussian function as the kernel.

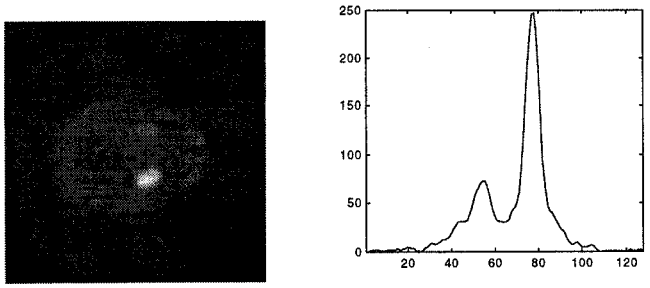

Figure 11. Reconstruction using the second method.

REFERENCES

[1] P. J. Early, and D. B. Sodee, *Principles and Practice of Nuclear Medicine*, 2nd ed., St. Louis: Mosby, 1995.

[2] J. A. Sorenson, and M. E. Phelps, *Physics in Nuclear Medicine*, Philadelphia: W. B. Sanders, 1987.

[3] L. van Elmbt, and S. Walrand, "Simultaneous correction of attenuation and distance-dependent resolution in SPECT: an analytical approach", *Phys. Med. Biol.*, vol. 38, 1207-1217, 1993.

[4] R. M. Lewitt, P. R. Edholm, and W. Xia, "Fourier method for correction of depth-dependent blurring", *SPIE Medical Imaging III*, vol. 1092, 232-243, 1989.

[5] Z. Liang, J. Ye, J. Cheng, and D. P. Harrington, "Analytical inversion for quantitative SPECT imaging including photon attenuation and resolution variation", Technical Report No. MICL-97-1, 1997.

[6] T. Inouye, K. Kose, and A. Hasegawa, "Image reconstruction algorithm for single-photon-emission computed tomography with uniform attenuation", *Phys. Med. Biol.*, vol. 34, 299-304, 1989.

[7] Z. Liang, J. Ye, J. Cheng, and D. P. Harrington, "The inversion of the exponential Radon transform for quantitative brain SPECT", *Phys. Med. Biol.*, vol. 41, 1227-1232, 1996.

[8] E. J. Soares, C. L. Byrne, S. J. Glick, C. R. Appedorn, and M. A. King, "Implementation and evaluation of an analytical solution to the photon attenuation and nonstationary resolution reconstruction problem in SPECT", *IEEE Trans Nucl. Sci.*, vol. 40, 1231-1237, 1993.

[9] X. Pan, and C. E. Metz, "Non-iterative methods and their noise characteristics in 2D SPECT image reconstruction", *IEEE Trans Nucl. Sci.*, vol. 44, 1388-1397, 1997.

[10] Z. Liang, J. Ye, and J. Cheng, "Quantitative brain SPECT in three dimensions: an analytical approach without transmission scans", P. Grangeat, and J. L. Amans eds., *Three-Dimensional Image Reconstruction in Radiology and Nuclear Medicine*, 117-132, 1996.

0-7803-5021-9/99/$10.00 (c) 1999 IEEE